JOURNAL OF AGRICULTURAL AND FOOD CHEMISTRY

pubs.acs.org/JAFC Article

Efficient Expression and Activity Optimization of Manganese Peroxidase for the Simultaneous Degradation of Aflatoxins AFB_1, AFB_2, AFG_1, and AFG_2

Yang Yang, Lina Sheng, Xueqing Hang, Jinyao Wang, Guocheng Kou, Yongli Ye, Jian Ji,* and Xiulan Sun

Cite This: J. Agric. Food Chem. 2025, 73, 1608−1618 Read Online

ACCESS | Metrics & More | Article Recommendations | Supporting Information

ABSTRACT: Aflatoxins (AFs), notorious mycotoxins that pose significant risks to human and animal health, make biodegradation extremely crucial as they offer a promising approach to managing and reducing their harmful impacts. In this study, we identified a manganese peroxidase from *Punctularia strigosozonata* (*Ps*Mnp) through protein similarity analysis, which has the capability to degrade four AFs (AFB_1, AFB_2, AFG_1, and AFG_2) simultaneously. The gene encoding this enzyme was subject to codon optimization, followed by cold shock induction expression using the pColdII vector, leading to the soluble expression of manganese peroxidase (Mnp) in *Escherichia coli*. This study tackled the problem of inclusion body formation that often occurs during Mnp expression in *E. coli*. After optimizing the degradation conditions, the degradation rates for AFB_1, AFB_2, AFG_1, and AFG_2 were 87.9, 72.8, 77.3, and 85.6%, respectively. Molecular docking and molecular dynamics simulations indicated that *Ps*Mnp facilitated the degradation of AFs through hydrophobic and polar interactions among various amino acid residues. This research offers novel insights into the rapid discovery of enzymes capable of degrading AFs and establishes a theoretical foundation for the efficient expression of mycotoxin detoxification enzymes.

KEYWORDS: *aflatoxins, manganese peroxidase, degradation, Escherichia coli, molecular dynamics*

1. INTRODUCTION

Aflatoxins (AFs), a highly toxic metabolite produced by fungi such as *Aspergillus flavus* and *Aspergillus parasite*, have emerged as a prominent concern in the field of food safety due to their profound impact on human and animal health and widespread global contamination.[1,2] The production of AFs is intricately linked to specific environmental conditions, with global warming exacerbating its occurrence.[3] Among the 18 identified AFs thus far, AFB_1, AFB_2, AFG_1, and AFG_2 stand out as the four most significant ones sharing similar chemical structures and possessing comparable toxic groups.[1] Notably, AFB_1 exhibits the highest toxicity and is classified as a Group I carcinogen by the International Agency for Research on Cancer.[4−6] AFs are relatively stable at high temperatures and their decomposition temperature is around 280 °C, which means that they maintain heat resistance within the conventional food processing temperature (80−121 °C).[7]

Physical, chemical, and biological methods have been developed to control AFB_1.[8,9] However, most physical and chemical approaches possess inherent limitations. Physical methods are time-consuming and can only achieve partial removal, while chemical methods significantly reduce AFB_1 concentration but result in inevitable loss of nutritional value in food and feed, along with high consumption costs.[10] Biological control offers a safe and effective approach for AFs elimination from food under mild conditions. Among the various biological detoxification methods (e.g., biological adsorption, microbial degradation), enzymatic degradation method is widely regarded as the most promising approach due to its exceptional efficiency.[11]

Many mycotoxin-degrading enzymes have been reported, such as redox enzyme, hydrolase, transferase, and carboxypeptidase.[12] Manganese peroxidase (Mnp, EC 1.11.1.13) stands out as a highly efficient biocatalyst with unique redox capabilities and remarkable substrate adaptability, thus garnering significant attention for its potential application in mycotoxin biodegradation.[13,14] Research indicates that multiple Mnps can degrade AFB_1 into AFB_1-8,9-epoxide, and safety assessments show that its toxicity is significantly lower than that of AFB_1.[15−17] Mnp is an extracellular glycosylated hemin protein belonging to the oxidoreductase family.[18] By utilizing H_2O_2 as an oxidant, Mnp effectively converts Mn^{2+} into Mn^{3+}.[19] However, it should be noted that the generated Mn^{3+} species are unstable but can form stable chelates with carboxylic acids.[20] These low molecular weight Mn^{3+}-organic acid chelates possess high redox potentials and can permeate through lignocellulosic structures as diffusing free radicals, thereby actively participating in the degradation of recalcitrant nonphenolic lignin structures and even disrupting aromatic rings within lignin polymers.[21] Certain mycotoxins may exhibit structural similarity to lignin monomers or their derivatives; for instance, AFB_1 possesses a coumarin structure, which is

Received: October 18, 2024
Revised: December 24, 2024
Accepted: December 24, 2024
Published: January 3, 2025

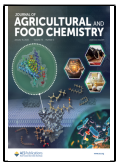

https://doi.org/10.1021/acs.jafc.4c10047
J. Agric. Food Chem. 2025, 73, 1608−1618

derived from the lignin monomer coumarin.[22] Previous studies have demonstrated the degradation of AFB_1 by laccase and Mnp.[23−26] Mnp exhibits a higher redox potential than laccase, indicating its superior capability to react with more recalcitrant substrates. Xia et al. effectively detoxified multiple mycotoxins using yeast-expressed Mnp.[27] However, compared to the expression system in *Escherichia coli*, yeast-based expression entails longer cycles, more intricate operations, and higher costs. While the *E. coli* expression system is advantageous due to its cost-effectiveness and rapid production capabilities, it has significant limitations concerning post-translational processing and modification. This often leads to target products being expressed as inclusion bodies, necessitating complex protein refolding procedures. Recently, research has shown successful expression of Mnp in *E. coli* systems that facilitate proper protein folding while preventing inclusion body formation.[17,28] This makes it possible to rapidly produce Mnp in *E. coli* expression systems.

The three-dimensional structure of mycotoxin-degrading enzymes can be efficiently and rapidly predicted using molecular docking and molecular dynamics techniques, which is pivotal for elucidating the catalytic mechanism of these enzymes.[29] With the rapid advancement of bioinformatics and computational chemistry, molecular docking and molecular dynamics have emerged as crucial methodologies for investigating the structure, function, and interactions of biomolecules. Molecular docking technology simulates the binding process between small molecules and biological macromolecules, predicting their binding mode and affinity while elucidating the mechanism and binding pathway of enzyme−substrate interactions. Previous studies have employed molecular predictions to investigate laccase-AF interactions.[30] On the other hand, molecular dynamics simulations provide insights into the relationship between structure and function by mimicking the dynamic behavior of biomolecules at an atomic level. This approach is frequently utilized to analyze enzyme−substrate stability during reaction processes. For instance, Peng et al. demonstrated how YKL069W mediates the degradation of patulin (PAT) to E-ascladiol using molecular dynamics simulation, elucidating the pivotal role of CYS125 and CYS101 as key amino acid residues in this process.[31]

In this study, the AF-degrading enzyme *Ceriporiopsis subvermispora* CsMnp (GenBank accession number: MG190336.1) was utilized as a template.[17] A *Ps*Mnp (GenBank: XP_007386962) derived from *Punctularia strigosozonata* was identified through a protein similarity comparison in the National Center for Biotechnology Information (NCBI) database. This protein exhibited significant effectiveness in degrading AFs. The codon of the gene encoding this enzyme was optimized and cold shock induced expression was performed using the pCold II vector. This approach resulted in the successful soluble expression of *Ps*Mnp in *E. coli*, addressing the issue of Mnp forming inclusion bodies when expressed in *E. coli*. Molecular dynamics simulation showed that the degradation of AFs was driven by the hydrophobic and polar interactions with *Ps*Mnp. This study offers a novel strategy for the mining and efficient expression of mycotoxin-degrading enzymes.

2. MATERIALS AND METHODS

2.1. Chemicals. The mycotoxins AFB_1, AFB_2, AFG_1, and AFG_2 were purchased from Pribolab (Qingdao, Shandong, China). In this work, AFB_1, AFB_2, and AFG_1, AFG_2 were dissolved in methanol to make a 1.0 mg/mL stock solution, and all the standard products were stored at −20 °C. TIANprep Rapid Mini Plasmid Kit was purchased from Tiangen Biotech (Beijing, China). Protein markers and protein loading buffers were purchased from Vazyme Biotech (Nanjing, China). His-tag Protein Purification Kit was purchased from Beyotime Biotechnology (Shanghai, China). PAGE Gel Fast Preparation Kit was purchased from EpiZyme Biotechnology (Shanghai, China). H_2O_2, 2,2′-azino-bis (3-ethylbenzothiazoline-6-sulfonic acid) (ABTS), and isopropyl-β-D-thiogalactopyranoside (IPTG) were purchased from Sigma-Aldrich (St. Louis, MO, USA). Methanol and acetonitrile were purchased from Thermo Fisher (Waltham, MA, USA). All the reagents and chemicals were of analytical reagent grade.

2.2. Sequence Analysis and Heterologous Expression. The amino acid sequences of known AFs-degrading enzymes were compared with the NCBI database using blastp, and the consistent sequences were selected as AFs-degrading enzyme candidates for mining. *Ps*Mnp was validated as a candidate degrading enzyme due to its high homology (82.54%) and unreported degradation of mycotoxins. The gene encoding *Ps*Mnp was optimized according to expression preference of *E. coli* and was synthesized by Tianlin Biotechnology Co., Ltd., Shanghai, China. The gene was cloned into pCold II with a 6x His affinity tag at the SacI and *Bam*HI restriction endonuclease cleavage sites. The pCold II-*Ps*Mnp plasmid was transfected into *E. coli* BL21(DE3) cells using the heat shock method. The strain was cultured in Luria−Bertani (LB) medium until reaching an OD_{600} value of 0.5. Subsequently, IPTG was added to induce protein expression at low temperatures, with continuous supplementation of $CaCl_2$ and hemin solution during the induction process. Bacterial cells were then harvested by centrifugation at 4 °C and 8000 rpm for 10 min. The obtained pellets were crushed by ultrasound to extract protein. The cell debris was then removed by centrifugation at 4 °C and 12,000 rpm for 10 min. Then, His-tag Protein Purification Kit was used to purify the *Ps*Mnp. Finally, the protein eluent was dialyzed in dialysate (PBS, pH 7.4) 5 times at 4 °C for 36 h. The concentration of *Ps*Mnp was determined by NANO-300 (Aosheng Instrument Co., Ltd., Hangzhou, China). The molecular weight of the purified *Ps*Mnp was analyzed by sodium dodecyl sulfate polyacrylamide gel electrophoresis (12%; SDS-PAGE) using a DYY-6D (Liuyi Biotechnology Co., Ltd., Beijing, China) type electrophoresis apparatus.

2.3. Determination of *Ps*Mnp Enzyme Activity. Mnp was dissolved in a 50 mM malonate buffer solution (1 mM ABTS, 1 mM $MnSO_4$ and 0.1 mM H_2O_2, pH 5.0). The enzyme activity was determined by measuring the oxidation rate of Mnp to 1 mM ABTS ($\varepsilon 420 = 36{,}000\ M^{-1}\cdot cm^{-1}$). The reaction was performed at 25 °C for 3 min and the detection wavelength was 420 nm. One unit (1 U) of Mnp activity was defined as the amount of enzyme required to generate 1 μmol of oxidation product per minute under standard conditions.[32]

2.4. Degradation of Four AFs by *Ps*Mnp. Mycotoxin degradation was carried out in a 50 mM malonate buffer solution at pH 5.0. The reaction system comprised 0.5 U/mL *Ps*Mnp, 1 mM $MnSO_4$, 0.1 mM H_2O_2, and a mixture of four AFs at a concentration of 1 μg/mL. The reaction was conducted at 30 °C for 60 h, with samples collected every 12 h. To terminate the reaction, an equal volume of methanol was added. Subsequently, the reaction mixture was filtered through a 0.22 μm organic filter.[33] The residual mycotoxin content was analyzed on an Agilent 1290 Infinity II Liquid Chromatograph coupled to an Agilent 6470 Triple Quadrupole Mass Spectrometer (Agilent Technologies Inc., California, USA). Each reaction was performed in triplicate.

2.5. Determination of Four AFs. The four AFs were determined using the Agilent 1290 Infinity II Liquid Chromatograph coupled to an Agilent 6470 Triple Quadrupole Mass Spectrometer (Agilent Technologies Inc., California, USA). The chromatographic column used was a BEH C18 (2.1 mm × 100 mm, 1.7 μm). The mobile phase A consisted of acetonitrile, while mobile phase B was an ammonium formate solution (10 mM). The column temperature was set at 45 °C, the flow rate was maintained at 0.3 mL/min, and the injection volume

https://doi.org/10.1021/acs.jafc.4c10047
J. Agric. Food Chem. 2025, 73, 1608−1618

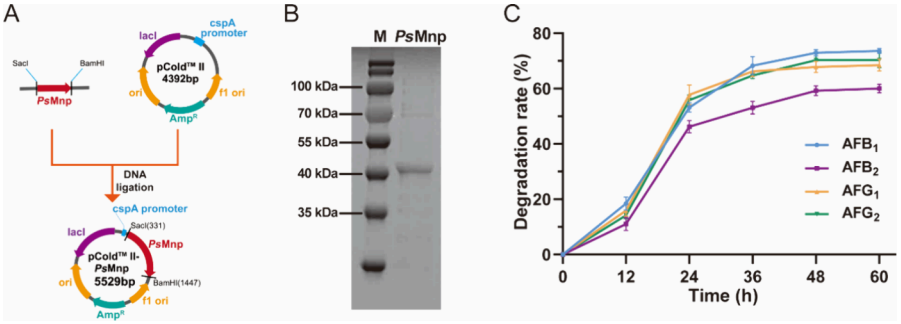

Figure 1. (A) Construction of pCold II-*Ps*Mnp. (B) SDS-PAGE analysis of *Ps*Mnp. Lane M: protein marker; lane *Ps*Mnp: purified *Ps*Mnp. (C) Time-dependent degradation effect of *Ps*Mnp on four AFs.

was 5 μL. The gradient elution conditions are detailed in Table S1. The mass spectrometry conditions employed an electrospray ionization (ESI) source, utilizing multiple reaction monitoring (MRM) in positive ion scan mode as the monitoring technique. The spray pressure was set at 0.21 MPa, and the drying gas flow rate was maintained at 8 L/min, with a temperature of 550 °C. The capillary voltage was established at 5,500 V. Detailed settings for the triple quadrupole ion pairs and associated voltage parameters are provided in Table S2. The standard curves for AFB_1, AFB_2, AFG_1, and AFG_2 are shown in Figure S1.

2.6. Optimization of Expression Conditions. The temperature, IPTG concentration, hemin concentration, and induction time were optimized. Recombinant strain *E. coli* BL21 (pCold II-*Ps*Mnp) was cultured in LB medium containing 100 μg/mL ampicillin until OD_{600} reached 0.5. The culture bottle was immersed in an ice bath and rapidly cooled to 6−14 °C, followed by oscillation at 180 rpm for 30 min at the same temperature. Subsequently, IPTG was added to the medium at a final concentration of 0.02−0.5 mM. The shaker was set to 180 rpm and temperature was maintained at 6−14 °C for 10−30 h. After adding IPTG for 6 h, $CaCl_2$ solution and hemin solution were gradually added to achieve final concentrations of 1 mM and 0.1−1.5 mM, respectively. The parameters were individually adjusted to optimize the expression levels of enzyme *Ps*Mnp, and subsequently, the enzymatic activity was used for characterization.

2.7. Optimization of Degradation Conditions. The optimal conditions for the degradation of four AFs by *Ps*Mnp were determined by optimizing pH, temperature, Mn^{2+} concentration, and H_2O_2 concentration. The degradation rates of the four AFs over a 36-h period were assessed within a pH range of 2.5−5, a temperature range of 20−70 °C, a Mn^{2+} concentration range of 0.1−5 mM, and an H_2O_2 concentration range of 0.05−2 mM.

2.8. 3-Dimensional (3D) Structure of *Ps*Mnp. The SWISS-MODEL (https://swissmodel.expasy.org/interactive) online software is used for protein tertiary structure prediction, which involves three main steps: template sequence identification, homology modeling, and model evaluation. The process begins by inputting the preprepared sequence, followed by an automatic search for template sequences. Templates with high similarities (typically above 50%) are selected to serve as the basis for homology modeling. Subsequently, the optimal model structure is chosen based on pull diagram analysis.

2.9. Molecular Docking of *Ps*Mnp and Four AFs. The molecular docking program employed in this experiment is AutoDock Vina (Version 1.2.3).[34,35] It employs the "Iterated Local Search" algorithm for continuous local search and repeated iteration to identify the optimal molecular docking conformation, selecting the scheme with the lowest binding energy as the final choice. Initially, three-dimensional structures of AFB_1, AFB_2, AFG_1, and AFG_2 were obtained from the PubChem database prior to docking. Subsequently, using AutoDock Tools software (Version 1.5.6), small molecules and proteins underwent preprocessing while an appropriate docking site was selected to generate a configuration file for AutoDock Vina software's docking process. The AutoDock Vina software then performed continuous local search and repeated iteration to discover the best molecular docking conformation. Finally, PyMOL (version 4.6.0) was utilized for result analysis and visualization.

2.10. Molecular Dynamics Simulation of *Ps*Mnp and Four AFs. Kinetic simulations of four protein-small molecule systems (AFB_1, AFB_2, AFG_1, and AFG_2) were conducted using GROMACS 2024. The geometry of the small molecule structures was optimized using Gaussian 16, and the electrostatic charges were calculated with Multiwfn software utilizing the RESP (Restricted Electrostatic Potential) fitting method at the B3LYP/6-31G(d) level. The results from the protein-small molecule docking served as the initial configuration for the dynamic simulations. Amber 03 force field parameters were assigned to proteins using GROMACS, and GAFF (Generalized Amber Force Field) parameters were constructed for small molecules using Sobtop tools.

The protein-small molecule complex was centrally positioned within a cubic box, with the solute maintained at a distance of 1.0 nm from the box edges. The model was solvated using the SPC (Simple Point Charge) water model, and appropriate amounts of sodium and chloride ions were added to ensure the system's electroneutrality. Energy minimization (EM) was conducted using the steepest descent algorithm. Subsequently, the solute was confined within an isothermal isovolumetric (NVT) ensemble, where the system was heated from 0 to 300 K, followed by equilibration at 300 K and 1 bar in an isothermal isobaric (NPT) ensemble. Finally, a 100 ns molecular dynamics simulation of the protein-small molecule complex was performed, and the simulation trajectory was saved for subsequent analysis. A truncation distance of 12 Å was employed for van der Waals interactions, while Coulomb interactions were managed using the Particle-Mesh Ewald (PME) method.

The results from the molecular dynamics (MD) simulation were analyzed using metrics such as root-mean-square deviation (RMSD), radius of gyration (R_g), hydrogen bonds (H-bonds), and binding energy. The local Gibbs free energy was calculated based on the RMSD and R_g values using the "g-sham" and "xpm2txt.py" scripts. The three-dimensional Gibbs free energy potential was visualized using Origin (2021, OriginLab, USA). Additionally, the "gmx-mmpbsa" script was employed to compute the molecular mechanics generalized Born surface area (MM/GBSA) method, allowing for the determination of the binding free energy between the small molecule and the protein at the target binding site, thereby assessing its thermodynamic stability.

2.11. Statistical Analysis. The data processing and analysis were performed using SPSS 26, and GraphPad Prism 8 was utilized for data visualization. All experiments were independently replicated, and the mean ± standard deviation of three replicates ($n = 3$) was graphically represented. A significance threshold of $p < 0.05$ was applied.

3. RESULTS AND DISCUSSION

3.1. Cloning, Expression, and Purification of *Ps*Mnp and Its Enzymatic Degradation Capability toward Four AFs. The coding gene for the *Ps*Mnp enzyme, which degrades AFB_1, was identified through blastp sequence alignment in the NCBI database. As illustrated in Figure 1A, the synthesized

https://doi.org/10.1021/acs.jafc.4c10047
J. Agric. Food Chem. 2025, 73, 1608−1618

*Ps*Mnp gene was cloned into the pColdII vector using SacI and *Bam*HI restriction enzyme sites, creating the pColdII-*Ps*Mnp plasmid. This plasmid was then introduced into *E. coli* BL21 (DE3) for heterologous expression. However, expressing fungal-derived peroxidases in *E. coli* often leads to the formation of inclusion bodies.[28] While reducing the induction temperature can sometimes yield soluble proteins, it may also reduce Mnp expression under the control of the T7 promoter.[36] To overcome this issue, cold-shock-controlled *csp*A promoters can be used to regulate protein expression.[37] In this study, *Ps*Mnp was successfully expressed as a soluble protein at low temperatures using the *csp*A promoter vector pColdII under IPTG induction conditions. The recombinant protein *Ps*Mnp, consisting of 378 amino acid residues, was predicted to have a molecular mass of approximately 39.5 kDa. Subsequent SDS-PAGE analysis of the purified *Ps*Mnp, as shown in Figure 1B, revealed a prominent band near the 40 kDa marker, which is consistent with the anticipated molecular weight. Hemin is a critical component of the active center of Mnp, playing a pivotal role in its catalytic mechanism. During the expression of *Ps*Mnp, additional supplementation of hemin at high concentrations was necessary. For instance, it has been reported that manganese peroxidase *Phc*Mnp from *Phanerochaete chrysosporium* exhibits the highest enzymatic activity of 19 U/mg at a hemin concentration of 1%.[38]

The chelation of manganese ions by malonic acid facilitates the formation of complexes with a high redox potential, thereby promoting the oxidation of Mn^{2+} to Mn^{3+} by Mnp and enhancing substrate oxidation.[32] Consequently, we selected the malonate buffer system for the degradation of AFs by *Ps*Mnp in this study (Figure 1C). After a 12-h reaction period, the degradation rates were 18.5% for AFB_1, 11.1% for AFB_2, 15.9% for AFG_1, and 14.2% for AFG_2. Extending the reaction time to 24 h led to a notable increase in degradation rates, reaching 53.1% for AFB_1, 46.3% for AFB_2, 57.8% for AFG_1, and 55.8% for AFG_2. Following a 36-h reaction period, degradation rates stabilized at 73.6, 60.1, 68.5, and 70.3% for AFB_1, AFB_2, AFG_1, and AFG_2, respectively. You et al. used *Phc*Mnp expressed by *Pichia pastoris* GS115 to degrade AFB1 at a rate of 76.56%.[38] After optimizing the enzyme induction expression conditions and reaction parameters, the degradation rate of AFB_1 by *Phc*Mnp increased by 11.42%. Therefore, further optimization of the induced expression conditions is imperative to augment the enzyme activity of *Ps*Mnp.

3.2. Optimization of Enzyme-Induced Expression Conditions of *Ps*Mnp. In order to optimize the induction conditions, we investigated the effects of temperature, IPTG concentration, hemoglobin addition, and induction time on enzyme activity (Figure 2A). The optimal expression temperature for *Ps*Mnp was determined to be 8 °C with an enzyme activity of 23.4 U/mg. Notably, increasing the temperature resulted in a significant decrease in enzyme activity. It is worth mentioning that *E. coli* cytoplasm lacks a suitable redox environment which often leads to the formation of inclusion bodies during Mnp expression.[17] Lowering the temperature can reduce folding stress and enhance the proteolytic activity of the target protein.[39]

The concentration of IPTG greatly affects protein expression by influencing the strength and efficiency of induction.[40] Low IPTG levels lead to weak activation of the lac promoter, resulting in lower target protein expression. On the other hand, high IPTG concentrations can stress the cells, trigger toxicity, hinder growth and protein solubility, and may even cause cell death.[41] As shown in Figure 2B, the optimal IPTG concentration for *Ps*Mnp expression was 0.2 mM, yielding an enzyme activity of 23.6 U/mg.

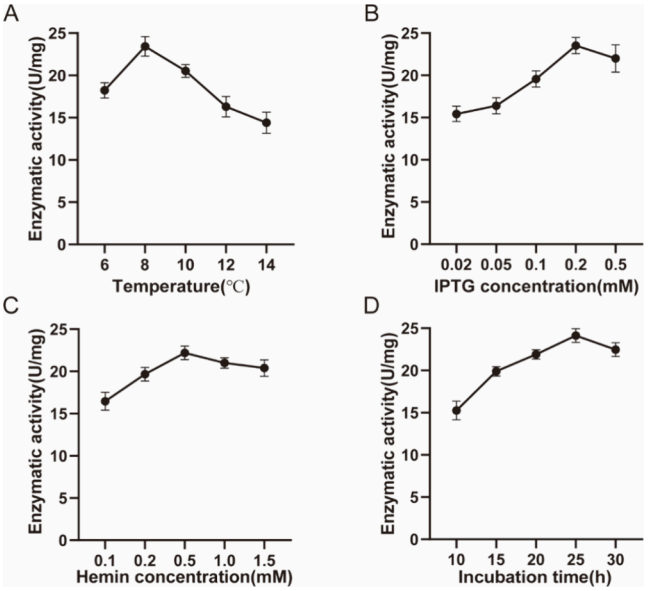

Figure 2. Study on optimizing conditions for inducing enzyme activity expression. (A) Impact of induction temperature on *Ps*Mnp enzyme activity. (B) Influence of IPTG concentration on *Ps*Mnp enzyme activity. (C) Effect of hemin concentration on *Ps*Mnp enzyme activity. (D) Influence of induction time on *Ps*Mnp enzyme activity.

hemin is a crucial component of the active center of Mnp and plays a key role in its catalytic activity. As illustrated in Figure 2C, the optimal activity of *Ps*Mnp was observed at a hemin concentration of 0.5 mM, yielding an enzyme activity of 22.2 U/mg. However, excessive hemin can reduce *Ps*Mnp activity, consistent with previous findings.[28]

The optimal duration of induction is crucial for achieving efficient protein expression. Induction time significantly affects protein expression levels, cell growth, and overall protein production. As shown in Figure 2D, variations in incubation times lead to notable differences in enzyme activity. After a 25-h induction period, *Ps*Mnp exhibited the highest enzyme activity, reaching 24.1 U/mg.

3.3. Optimization of Degradation Conditions of Four AFs by *Ps*Mnp. The activity of enzymes is influenced by various factors. To identify the optimal reaction conditions, we assessed the degradation efficiency of AFs by *Ps*Mnp under different environmental conditions. Specifically, we investigated the effects of pH, temperature, and concentrations of Mn^{2+} and H_2O_2 on degradation efficiency.

As shown in Figure 3A, the degradation results for AFB_1, AFB_2, AFG_1, and AFG_2 at various pH levels indicate that the highest degradation rates—86.9, 71.8, 70.5, and 81.7%, respectively—occur at a pH of 4.0. A slight decrease in degradation rates was observed at a pH of 4.5. However, when the pH fell below 4.0 or exceeded 4.5, degradation rates exhibited significant variations, suggesting that the optimal pH range for *Ps*Mnp in degrading the four AFs is between 4.0 and 4.5.

Temperature also plays a critical role in enzyme activity, with significant implications for catalytic efficiency, as illustrated in Figure 3B. The degradation efficiency of *Ps*Mnp against AFs increased notably with rising temperatures,

https://doi.org/10.1021/acs.jafc.4c10047
J. Agric. Food Chem. 2025, 73, 1608−1618

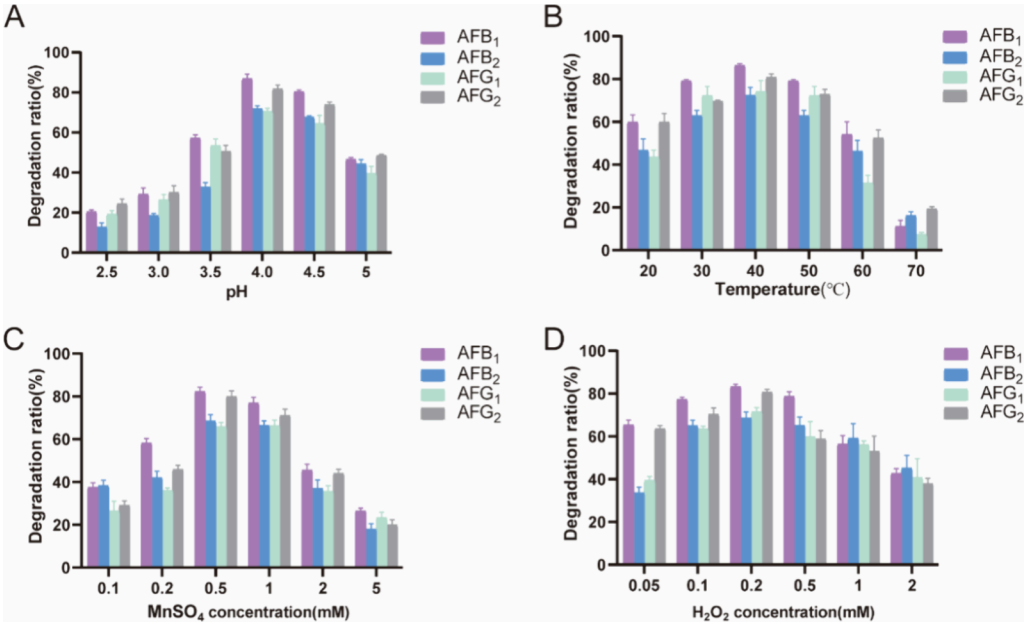

Figure 3. Optimal reaction parameters for the degradation of four AFs by *Ps*Mnp. (A) Impact of pH on the AF degradation rate. (B) Influence of temperature on the degradation rate of AFs. (C) Concentration effect of $MnSO_4$ on the rate of AF degradation. (D) Concentration effect of H_2O_2 on the degradation rate of AFs.

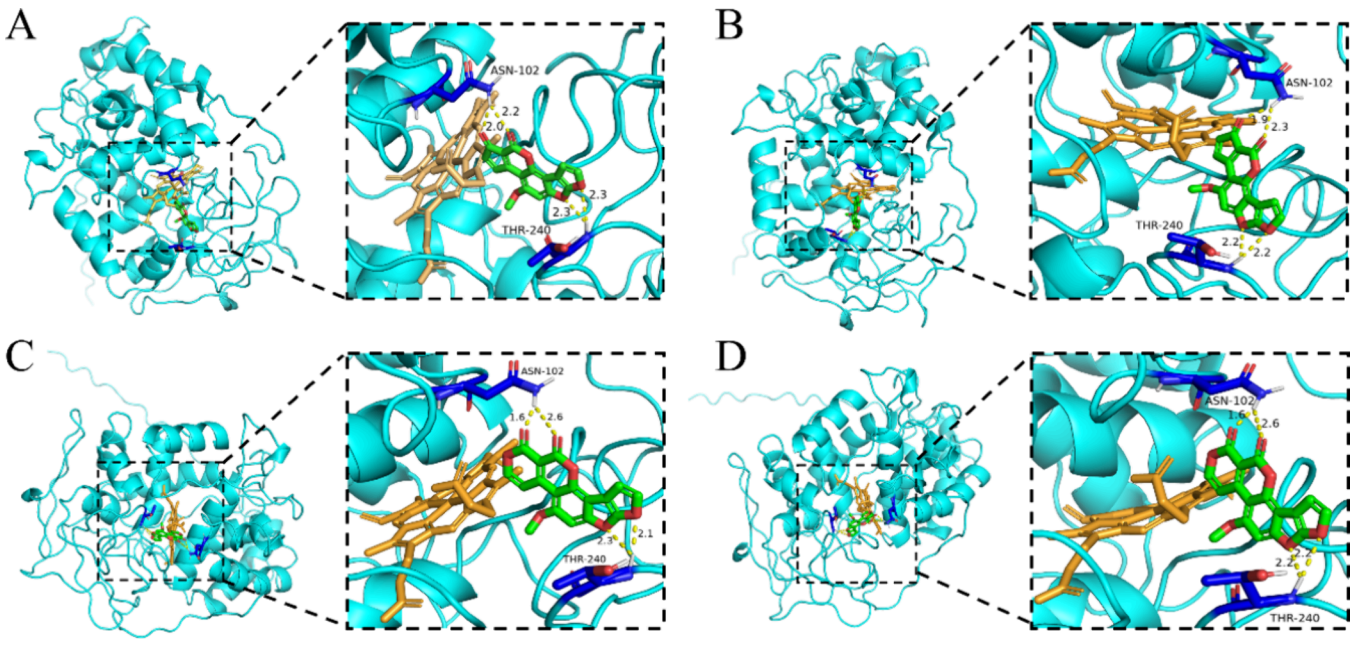

Figure 4. Molecular docking analysis was performed to investigate the interaction between *Ps*Mnp and four AFs. (A) Interaction model of AFB_1 with *Ps*Mnp. (B) Interaction model of AFB_2 with *Ps*Mnp. (C) Interaction model of AFG_1 with *Ps*Mnp. (D) Interaction model of AFG_2 with *Ps*Mnp. The AF molecules are depicted in green, hemin molecules in dark yellow, and hydrogen bonds as light dashed yellow lines. The numerical values represent the distance of interaction between amino acid residues and AF.

peaking at 40 °C. At this temperature, the degradation rates for AFB_1, AFB_2, AFG_1, and AFG_2 reached 86.3, 72.4, 74.2, and 80.8%, respectively. Notably, the degradation efficiency of *Ps*Mnp remained relatively stable within a temperature range of 30−50 °C, demonstrating the enzyme's capacity to maintain high activity over a broad thermal spectrum. This characteristic is particularly advantageous for the application of *Ps*Mnp in the food and feed industries.

In addition to pH and temperature, Mn^{2+} and H_2O_2 are critical components in this catalytic reaction system. *Ps*Mnp requires these elements to enhance the redox potential, thereby facilitating more effective degradation of AFs.[42] As shown in Figure 3C,D, the degradation efficiency of AFs initially increased with rising concentrations of Mn^{2+} and H_2O_2, before subsequently declining. The highest degradation efficiencies for *Ps*Mnp were observed at a $MnSO_4$ concentration of 0.5 mM, achieving 82.3% for AFB_1, 68.5% for AFB_2, 65.9% for AFG_1, and 79.9% for AFG_2. When the concentration exceeded 1 mM, the degradation rates decreased significantly, likely due to the inhibitory effects of excess Mn^{2+} on the enzymatic

https://doi.org/10.1021/acs.jafc.4c10047
J. Agric. Food Chem. 2025, 73, 1608−1618

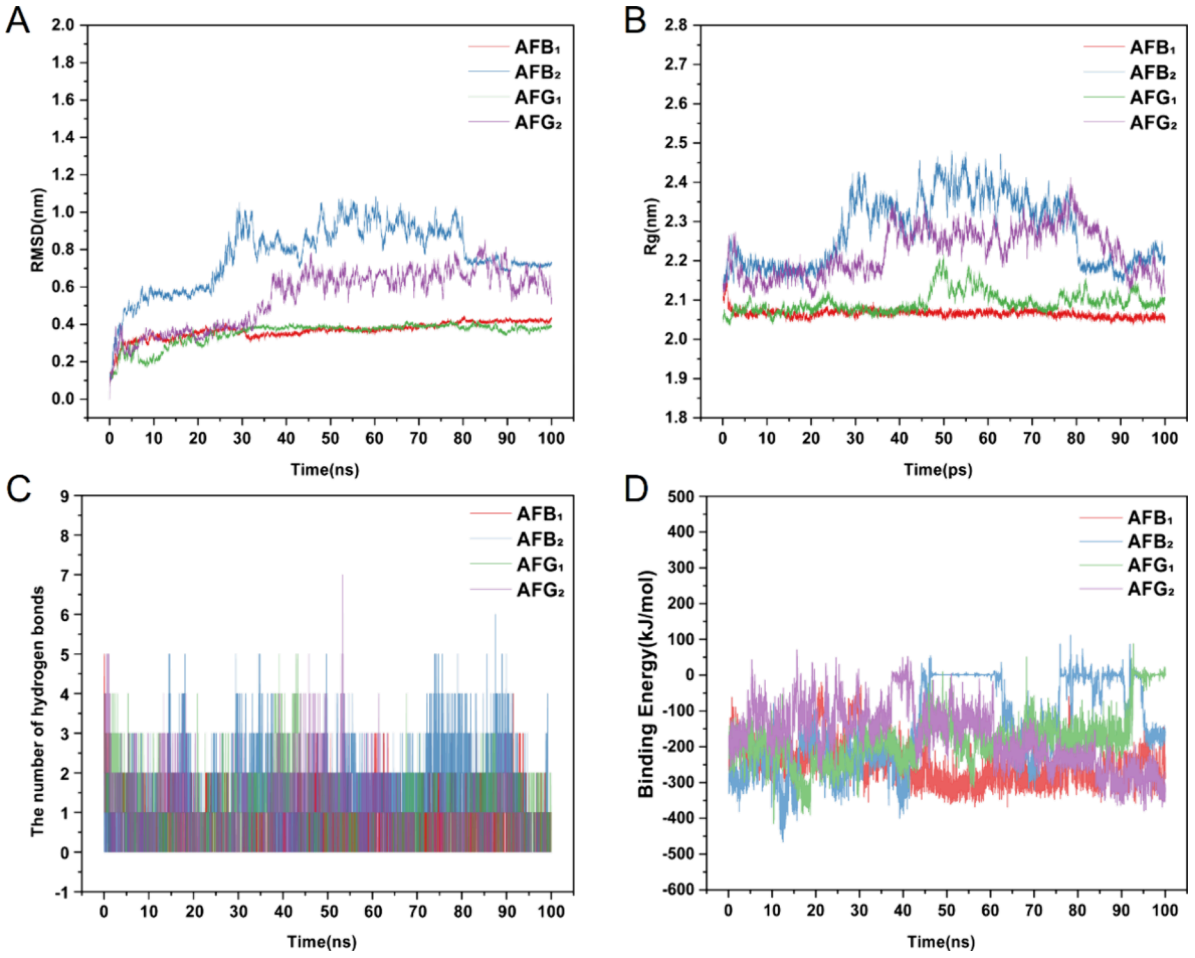

Figure 5. Kinetic simulation results of the complexes *Ps*Mnp-AFB_1, *Ps*Mnp-AFB_2, *Ps*Mnp-AFG_1, and *Ps*Mnp-AFG_2. (A) Root-mean-square deviation (RMSD), (B) radius of gyration (R_g), (C) number of hydrogen bonds, and (D) binding energy curve.

activity of *Ps*Mnp.[43] At an H_2O_2 concentration of 0.2 mM, the degradation efficiencies for AFB_1, AFB_2, AFG_1, and AFG_2 reached their maximum values of 83.3, 68.5, 71.6, and 80.7%, respectively.

In conclusion, the degradation experiments conducted under optimized conditions achieved efficiencies of 87.9% for AFB_1, 72.8% for AFB_2, 77.3% for AFG_1, and 85.6% for AFG_2 with *Ps*Mnp. Compared to the nonoptimized conditions, these values reflect significant increases of 14.3, 12.7, 8.8, and 15.3% for AFB_1, AFB_2, AFG_1, and AFG_2, respectively.

Mnp has garnered increased interest for its potential industrial applications, particularly in the treatment of agricultural waste and lignin degradation.[44] Some mycotoxins possess structures similar to lignin monomers or their derivatives,[45] indicating that these mycotoxins may also be amenable to degradation by manganese peroxidase. For instance, recombinant *Phc*Mnp expressed in *Kluyveromyces lactis* demonstrated an AFB_1 degradation rate of up to 75.71%.[46] Furthermore, You et al. expressed *Phc*Mnp in *Pichia pastoris*, and after optimizing the expression conditions, the degradation rate of AFB_1 was increased to 85.31%.[38] *Ps*Mnp can be expressed in *E. coli* to achieve comparable or better degradation effects. Unlike yeast expression systems, the *E. coli* expression system offers advantages such as ease of operation, rapid growth rates, lower culture costs, and higher expression yields, which enhance the cost-effectiveness of mycotoxin-degrading enzymes.[47] Although recombinant *Cs*Mnp in *E. coli* can achieve a degradation effect of up to 90%, its reaction time to reach this plateau is 72 h, significantly exceeding the reaction time of *Ps*Mnp for degrading aflatoxins.[33] In practical applications, Mnp that are lower in cost, more efficient, and faster in conversion speed are preferred. Considering the strict limits on H_2O_2 concentration in food and feed, current research has utilized glucose oxidase in reaction systems to oxidize glucose and release H_2O_2, rather than adding it directly.[15] Therefore, the recombinant strain of *E. coli* and *Ps*Mnp constructed in this study have good application potential in the field of mycotoxin control.

3.4. Molecular Docking Simulation of *Ps*Mnp Degradation of AFs. As shown in Table S3 and Figure S2, Ramachandran plot analysis indicated that 94% of the *Ps*Mnp residues were situated within the allowed region, suggesting that our *Ps*Mnp homology model is suitable for stereochemical binding studies with AFs. Consequently, we conducted docking simulations between the *Ps*Mnp homology model and AFB_1, AFB_2, AFG_1, and AFG_2. hemin acts as a crucial cofactor for MnP and is vital for its catalytic function. Therefore, prior to investigating the interactions between *Ps*Mnp and the AFs, we first assessed the interactions between hemin molecules and *Ps*Mnp to establish a *Ps*Mnp-hemin complex (Figure S3).

As shown in Figure 4, all four AFs formed two hydrogen bonds with the amino acid residues ASN-102 and THR-240, which are located near the hemin in *Ps*Mnp. These specific

https://doi.org/10.1021/acs.jafc.4c10047
J. Agric. Food Chem. 2025, 73, 1608−1618

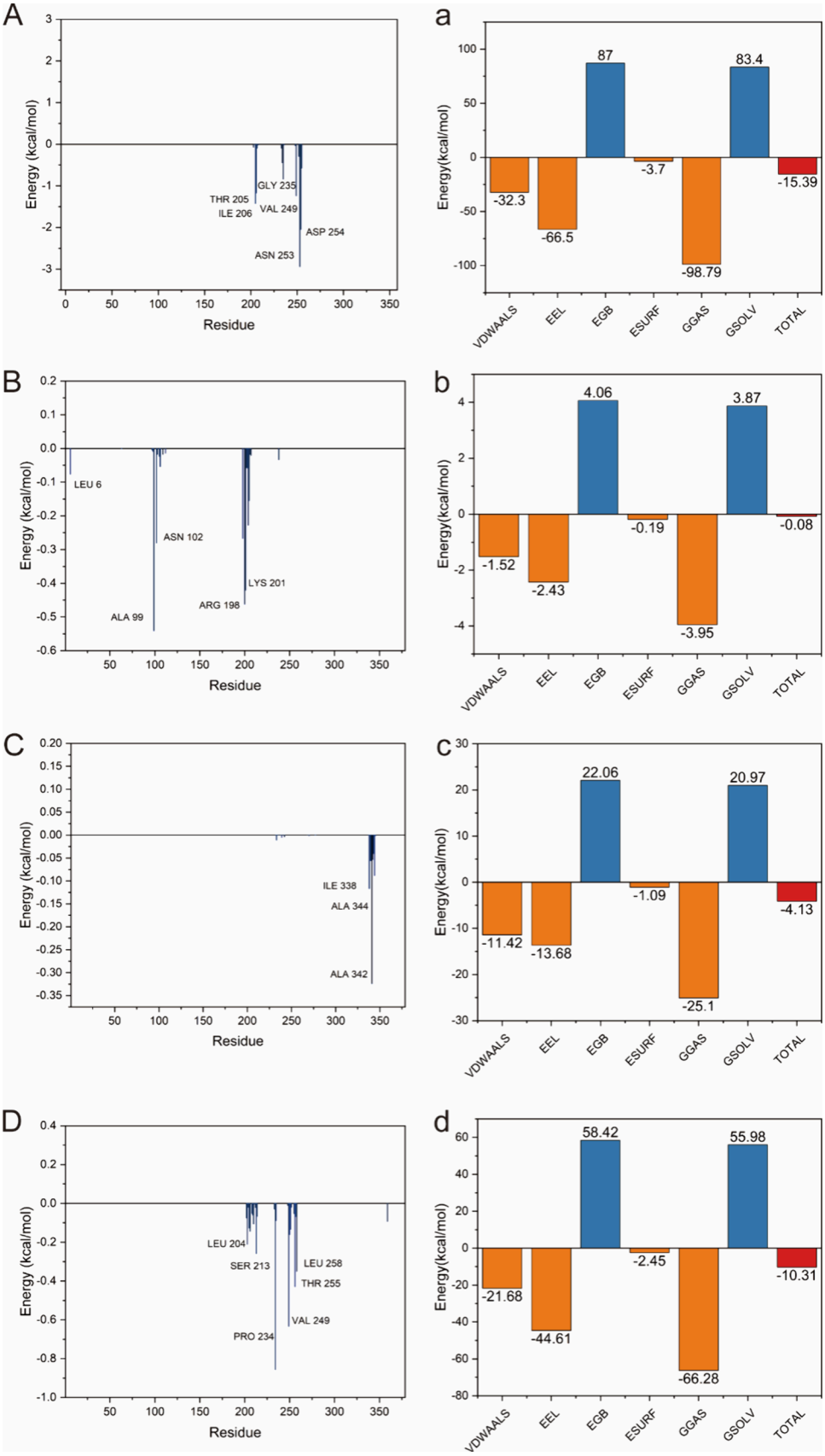

Figure 6. (A–D) Contribution of specific amino acids to the overall binding energy. (a–d) Small molecular-protein binding free energy decomposition diagram. VDWAALS, EEL, EGB, ESURF, GGAS, GSOLV, and TOTAL represent van der Waals force, electrostatic energy polar solvation energy, generalized Born electrostatic solvation energy, surface solvation energy, gas phase energy, solvation energy term, and average binding free energy, respectively. (A, a) AFB_1, (B, b) AFB_2, (C, c) AFG_1, and (D, d) AFG_2.

https://doi.org/10.1021/acs.jafc.4c10047
J. Agric. Food Chem. 2025, 73, 1608–1618

residues are critical for mediating the interaction between *Ps*Mnp and its substrates.[30] As presented in Table S4, slight variations in the molecular interaction scores of each AF with *Ps*Mnp may be attributed to their chemical similarities. Distinct binding affinities are likely to result in diverse ligand-*Ps*Mnp binding patterns. Notably, AFB_1 exhibited the highest binding capacity among all the AFs interacting with *Ps*Mnp, followed by AFG_1, AFB_2, and AFG_2, consistent with the degradation results.

3.5. Molecular Dynamics Simulation of *Ps*Mnp Degradation of AFs. The conformational changes in the *Ps*Mnp-AFB_1, *Ps*Mnp-AFB_2, *Ps*Mnp-AFG_1, and *Ps*Mnp-AFG_2 complexes were analyzed through molecular dynamics simulations to assess their stability. The RMSD was used to evaluate the balance and flexibility of the complexes.[48] As shown in Figure 5A, the RMSD results indicate that the complex structures of *Ps*Mnp-AFB_1 and *Ps*Mnp-AFG_1 exhibit only slight fluctuations after 20 ns, generally remaining low throughout the 100 ns simulation before achieving stability. The RMSD of the *Ps*Mnp-AFG_2 complex stabilized within a specific range after 40 ns. In contrast, the RMSD value for *Ps*Mnp-AFB_2 was higher and more variable, eventually stabilizing around 0.7 nm after 80 ns. This analysis suggests that *Ps*Mnp demonstrates greater stability in the catalytic degradation of AFB_1 and AFG_1 compared to AFB_2 and AFG_2.

The radius of gyration (R_g) was used to determine the compactness of the complexes. Figure 5B shows that both *Ps*Mnp-AFB_1 and *Ps*Mnp-AFG_1 exhibit low R_g fluctuations, consistent with their relatively stable RMSD trends. Conversely, the R_g value of *Ps*Mnp-AFB_2 decreased significantly during the later stages of the simulation, aligning with the structural changes observed in the RMSD and potentially indicating a relative shift or dissociation of the small molecule from the protein. It is important to note that while RMSD and R_g provide reference metrics for structural changes during the simulation, they do not directly correlate with the final binding energy of the receptor−ligand interactions.[49]

The number of hydrogen bonds serves as a reliable indicator of the stability of protein−ligand interactions. As depicted in Figure 5C, AFB_1 maintained a consistent number of hydrogen bonds with the protein throughout the simulation, which played a crucial role in stabilizing the binding complex. Binding energy analysis further revealed that AFB_1 exhibited the best binding energy, followed by AFG_2, indicating a relatively strong and stable interaction with the protein. In contrast, AFB_2 demonstrated poor binding energy, notably recording zero binding energy during two intervals (Figure 5D). This finding reflects the instability of its interaction with the protein and suggests potential complete dissociation during those periods.

The molecular mechanics energies combined with generalized Born and surface area continuum (MM-GBSA) solvation calculation is a method utilized to assess the stability and thermodynamic parameters of protein−ligand interactions. Through energy decomposition analysis, we can quantitatively evaluate the contributions of specific amino acid residues to ligand binding, which is crucial for elucidating the key determinants of molecular recognition.

As illustrated in Figure 6A, the simulation system involving AFB_1 identified THR 205, GLY 235, ILE 206, VAL 249, and ASN 253 as the primary residues contributing to energy. Notably, the significant negative energy contributions from GLY 235 and VAL 249 indicate that these residues are critical for the interaction between *Ps*Mnp and AFB_1. The energy composition analysis shows that the total energy contribution of the system is −15.39 kcal/mol, with van der Waals interactions and the GBSA being the most significant contributors to the binding energy. This indicates that the binding of AFB_1 is predominantly driven by hydrophobic and polar interactions. In the molecular dynamics system involving AFB_2, the energy contributions of ALA 99, ASN 102, and ARG 198 are relatively significant, as shown in Figure 6B. The negative energy contributions from ASN 102 and ARG 198 underscore the crucial role of these polar residues in the binding of AFB_2. The total binding energy is −0.08 kcal/mol, which may be attributed to the dissociation of AFB_2 from the binding pocket of *Ps*Mnp. This helps explain the low degradation efficiency of AFB_2 by *Ps*Mnp.

In the AFG_1 simulations, the residues ILE 338, ALA 344, and ALA 342 exhibit significant negative energy contributions, as depicted in Figure 6C. Notably, the substantial contribution of ALA 344 highlights its essential role in maintaining structural stability. The total energy of the system was −4.13 kcal/mol. In the simulation of AFG_2 (Figure 6D), the residues LEU 204, SER 213, THR 255, VAL 249, and PRO 234 exhibit significant energy contributions. The hydrophobic characteristics of these residues contribute to the stabilization of the ligands. The total binding energy for AFG_2 is −10.31 kcal/mol, which is lower than that of AFG_1. This indicates that the ligand-protein interactions are tighter and more stable in the AFG_2 system. Consequently, this may explain why the degradation rate of AFG_1 is slightly lower than that of AFG_2.

In summary, this study screened an enzyme capable of degrading AFs, *Ps*Mnp, from the NCBI database and constructed the enzyme using the pColdII expression vector. The enzyme was successfully induced for soluble expression in *E. coli* at low temperatures using the *csp*A promoter, achieving an enzyme activity of 24.1 U/mg after optimization of the induction conditions. *Ps*Mnp demonstrated significant degradation effects on AFs. By optimizing the degradation conditions, the highest degradation rate of *Ps*Mnp was achieved at a pH of 4.0, a degradation temperature of 40 °C, a MnSO4 concentration of 0.5 mM, and an H_2O_2 concentration of 0.2 mM. Under these conditions, the degradation rates for AFB_1, AFB_2, AFG_1, and AFG_2 were 87.9, 72.8, 77.3, and 85.6%, respectively. Additionally, molecular docking studies indicated that AFB_1, AFB_2, AFG_1, and AFG_2 could effectively bind to *Ps*Mnp, with respective binding energies of −8.24, −7.61, −8.03, and −7.18 kcal/mol. Molecular dynamic simulations showed that *Ps*Mnp and AFs binding was mainly driven by hydrophobic and polar interactions. This indicates that the application of *Ps*Mnp in the prevention and control of mycotoxins has great potential. However, the maturity and reliability of degrading enzymes in practical applications remain a challenge, as their stability and activity may be influenced by various factors present in foods and feeds. Protein engineering and enzyme immobilization techniques will facilitate the expansion of the expression and application of degradative enzymes.

■ ASSOCIATED CONTENT

Supporting Information

The Supporting Information is available free of charge at https://pubs.acs.org/doi/10.1021/acs.jafc.4c10047.

https://doi.org/10.1021/acs.jafc.4c10047
J. Agric. Food Chem. 2025, 73, 1608−1618

Elution gradient of the mobile phase for AF detection (Table S1); detailed listing of specific ions for each toxin for AF detection (Table S2); 3−homology modeling of *Ps*Mnp (Table S3); docking score of molecules binding to *Ps*Mnp (Table S4); standard curves of AFB_1, AFB_2, AFG_1, and AFG_2 (Figure S1); homology models of *Ps*Mnp protein sequences and Ramachandran plot (Figure S2); and homology models of *Ps*Mnp-hemin protein sequences (Figure S3) (PDF)

AUTHOR INFORMATION

Corresponding Author

Jian Ji − *School of Food Science and Technology, International Joint Laboratory on Food Safety, Synergetic Innovation Center of Food Safety and Quality Control, Jiangnan University, Wuxi, Jiangsu 214122, P.R. China; Key Laboratory of Screening, Prevention, and Control of Food Safety Risks, State Administration for Market Regulation, Wuxi, Jiangsu 214122, P.R. China; Institute of Future Food Technology, JITRI, Yixing 214200, China;* orcid.org/0000-0001-9405-1084; Phone: +86 510-85329015; Email: jijian@jiangnan.edu.cn; Fax: +86 85328726

Authors

Yang Yang − *School of Food Science and Technology, International Joint Laboratory on Food Safety, Synergetic Innovation Center of Food Safety and Quality Control, Jiangnan University, Wuxi, Jiangsu 214122, P.R. China; Key Laboratory of Screening, Prevention, and Control of Food Safety Risks, State Administration for Market Regulation, Wuxi, Jiangsu 214122, P.R. China; Institute of Future Food Technology, JITRI, Yixing 214200, China*

Lina Sheng − *School of Food Science and Technology, International Joint Laboratory on Food Safety, Synergetic Innovation Center of Food Safety and Quality Control, Jiangnan University, Wuxi, Jiangsu 214122, P.R. China; Key Laboratory of Screening, Prevention, and Control of Food Safety Risks, State Administration for Market Regulation, Wuxi, Jiangsu 214122, P.R. China; Institute of Future Food Technology, JITRI, Yixing 214200, China*

Xueqing Hang − *Institute of Future Food Technology, JITRI, Yixing 214200, China*

Jinyao Wang − *School of Food Science and Technology, International Joint Laboratory on Food Safety, Synergetic Innovation Center of Food Safety and Quality Control, Jiangnan University, Wuxi, Jiangsu 214122, P.R. China; Key Laboratory of Screening, Prevention, and Control of Food Safety Risks, State Administration for Market Regulation, Wuxi, Jiangsu 214122, P.R. China; Institute of Future Food Technology, JITRI, Yixing 214200, China*

Guocheng Kou − *School of Food Science and Technology, International Joint Laboratory on Food Safety, Synergetic Innovation Center of Food Safety and Quality Control, Jiangnan University, Wuxi, Jiangsu 214122, P.R. China; Key Laboratory of Screening, Prevention, and Control of Food Safety Risks, State Administration for Market Regulation, Wuxi, Jiangsu 214122, P.R. China*

Yongli Ye − *School of Food Science and Technology, International Joint Laboratory on Food Safety, Synergetic Innovation Center of Food Safety and Quality Control, Jiangnan University, Wuxi, Jiangsu 214122, P.R. China; Key Laboratory of Screening, Prevention, and Control of Food Safety Risks, State Administration for Market Regulation, Wuxi, Jiangsu 214122, P.R. China; Institute of Future Food Technology, JITRI, Yixing 214200, China*

Xiulan Sun − *School of Food Science and Technology, International Joint Laboratory on Food Safety, Synergetic Innovation Center of Food Safety and Quality Control, Jiangnan University, Wuxi, Jiangsu 214122, P.R. China; Key Laboratory of Screening, Prevention, and Control of Food Safety Risks, State Administration for Market Regulation, Wuxi, Jiangsu 214122, P.R. China; Institute of Future Food Technology, JITRI, Yixing 214200, China;* orcid.org/0000-0003-1528-8601

Complete contact information is available at: https://pubs.acs.org/10.1021/acs.jafc.4c10047

Author Contributions

Y.Y.: conceptualization, methodology, validation, data curation, writing—original draft. L.S.: investigation, writing—review and editing. X.H., J.W., and G.K.: data curation. Y.Y.: methodology, writing—review and editing. J.J.: project administration. X.S.: conceptualization, supervision.

Notes

The authors declare no competing financial interest.

ACKNOWLEDGMENTS

This work was financially supported by the National Key Research and Development Program of China (2022YFF1100703); the Key Laboratory of Biotoxin Analysis and Assessment for State Market Regulation (BAA202402); the Postgraduate Research and Practice Innovation Program of Jiangsu Province(KYCX24_2630); the Fundamental Research Funds for the Central Universities (JUSRP222001 and JUSRP123046); and Collaborative Innovation Center of Food Safety and Quality Control in Jiangsu Province, Jiangnan University.

REFERENCES

(1) Frisvad, J. C.; Hubka, V.; Ezekiel, C. N.; Hong, S. B.; Nováková, A.; Chen, A. J.; Arzanlou, M.; Larsen, T. O.; Sklenář, F.; Mahakarnchanakul, W.; Samson, R. A.; Houbraken, J. Taxonomy of Aspergillus section Flavi and their production of aflatoxins, ochratoxins and other mycotoxins. *Stud Mycol* **2019**, *93*, 1−63.

(2) Gao, Y. N.; Wang, Z. W.; Su, C. Y.; Wang, J. Q.; Zheng, N. Omics analysis revealed the intestinal toxicity induced by aflatoxin B1 and aflatoxin M1. *Ecotoxicol Environ. Saf* **2024**, *278*, No. 116336.

(3) Casu, A.; Camardo Leggieri, M.; Toscano, P.; Battilani, P. Changing climate, shifting mycotoxins: A comprehensive review of climate change impact on mycotoxin contamination. *Compr Rev. Food Sci. Food Saf* **2024**, *23* (2), No. e13323.

(4) Ostry, V.; Malir, F.; Toman, J.; Grosse, Y. Mycotoxins as human carcinogens-the IARC Monographs classification. *Mycotoxin Res.* **2017**, *33* (1), 65−73.

(5) Turner, N. W.; Subrahmanyam, S.; Piletsky, S. A. Analytical methods for determination of mycotoxins: a review. *Anal. Chim. Acta* **2009**, *632* (2), 168−180.

(6) Marin, S.; Ramos, A. J.; Cano-Sancho, G.; Sanchis, V. Mycotoxins: occurrence, toxicology, and exposure assessment. *Food Chem. Toxicol.* **2013**, *60*, 218−237.

(7) Stadler, D.; Berthiller, F.; Suman, M.; Schuhmacher, R.; Krska, R. Novel analytical methods to study the fate of mycotoxins during thermal food processing. *Anal Bioanal Chem.* **2020**, *412* (1), 9−16.

(8) Peng, Z.; Zhang, Y.; Ai, Z.; Pandiselvam, R.; Guo, J.; Kothakota, A.; Liu, Y. Current physical techniques for the degradation of aflatoxins in food and feed: Safety evaluation methods, degradation mechanisms and products. *Compr Rev. Food Sci. Food Saf* **2023**, *22* (5), 4030−4052.

(9) Peng, Z.; Chen, L.; Zhu, Y. Current major degradation methods for aflatoxins: A review. *Trends Food Sci. Technol.* **2018**, *80*, 155−166.
(10) Qiu, T.; Wang, H.; Yang, Y.; Yu, J.; Sun, X. Exploration of biodegradation mechanism by AFB1-degrading strain Aspergillus niger FS10 and its metabolic feedback. *Food Control* **2021**, *121* (2), No. 107609.
(11) Zhang, H.; Cui, L.; Xie, Y.; Li, X.; Zhao, R.; Yang, Y.; Sun, S.; Li, Q.; Ma, W.; Jia, H. Characterization, Mechanism, and Application of Dipeptidyl Peptidase III: An Aflatoxin B1-Degrading Enzyme from Aspergillus terreus HNGD-TM15. *J. Agric. Food Chem.* **2024**, *72*, 15998−16009.
(12) Ji, C.; Fan, Y.; Zhao, L. Review on biological degradation of mycotoxins. *Animal Nutrition* **2016**, *2* (3), 127−133.
(13) Zhang, S.; Dong, Z.; Shi, J.; Yang, C.; Fang, Y.; Chen, G.; Chen, H.; Tian, C. Enzymatic hydrolysis of corn stover lignin by laccase, lignin peroxidase, and manganese peroxidase. *Bioresour. Technol.* **2022**, *361*, No. 127699.
(14) Su, X.; Wang, S.; Wang, X.; Ji, W.; Zhang, H.; Tu, T.; Hakulinen, N.; Luo, H.; Bin, Y.; Zhang, W.; Huang, H. Targeting deoxynivalenol for degradation by a chimeric manganese peroxidase/glutathione system. *Ecotoxicol. Environ. Saf.* **2024**, *273*, No. 116130.
(15) Xia, Y.; He, R.; Sun, Y.; Zhou, H.; Gao, M.; Hu, X.; Cui, X.; Cheng, Q.; Wang, Z. Food-Grade Expression of Manganese Peroxidases in Recombinant Kluyveromyces lactis and Degradation of Aflatoxin B(1) Using Fermentation Supernatants. *Front Microbiol* **2022**, *12*, No. 821230.
(16) Wang, J.; Ogata, M.; Hirai, H.; Kawagishi, H. Detoxification of aflatoxin B1 by manganese peroxidase from the white-rot fungus Phanerochaete sordida YK-624. *FEMS Microbiology Letters* **2011**, *314* (2), 164−169.
(17) Wang, X.; Qin, X.; Hao, Z.; Luo, H.; Yao, B.; Su, X. Degradation of Four Major Mycotoxins by Eight Manganese Peroxidases in Presence of a Dicarboxylic Acid. *Toxins* **2019**, *11* (10), 566.
(18) Gold, M. H.; Alic, M. Molecular biology of the lignin-degrading basidiomycete Phanerochaete chrysosporium. *Microbiological reviews* **1993**, *57* (3), 605−622.
(19) Rahul, D.; Aditi, K.; Divyashri, B.; Ali, M.; Amitava, M.; Ram, M.; Pavel, F. Enzymatic Degradation of Lignin in Soil: A Review. *Sustainability* **2017**, *9* (7), 1163.
(20) Kondo, R.; Harazono, K.; Sakai, K. Bleaching of Hardwood Kraft Pulp with Manganese Peroxidase Secreted from Phanerochaete sordida YK-624. *Appl. Environ. Microbiol.* **1996**, *62* (12), 913−917.
(21) Zhang, H.; Zhang, X.; Geng, A. Expression of a novel manganese peroxidase from Cerrena unicolor BBP6 in Pichia pastoris and its application in dye decolorization and PAH degradation. *Biochemical Engineering Journal* **2020**, *153*, No. 107402.
(22) Guan, S.; Ji, C.; Zhou, T.; Li, J.; Ma, Q. Aflatoxin B(1) degradation by Stenotrophomonas maltophilia and other microbes selected using coumarin medium. *Int. J. Mol. Sci.* **2008**, *9* (8), 1489−1503.
(23) Mangini, V.; Rosini, E.; Caliandro, R.; Mangiatordi, G. F.; Delre, P.; Sciancalepore, A. G.; Pollegioni, L.; Haidukowski, M.; Mazzorana, M.; Sumarah, M. W. DypB peroxidase for aflatoxin removal: New insights into the toxin degradation process. *Chemosphere* **2024**, *349*, No. 140826.
(24) Marimon Sibaja, K. V.; de Oliveira Garcia, S.; Feltrin, A. C. P.; Remedi, R. D. Aflatoxin Biotransformation by commercial peroxidase and its application in contaminated food. *J. Chem. Technol. Biotechnol.* **2019**, *94*, 1187−1194.
(25) Bian, L.; Zheng, M.; Chang, T.; Zhou, J.; Zhang, C. Degradation of Aflatoxin B1 by recombinant laccase extracellular produced from Escherichia coli. *Ecotoxicology and environmental safety* **2022**, *244*, No. 114062.
(26) Loi, M.; De Leonardis, S.; Ciasca, B.; Paciolla, C.; Mulè, G.; Haidukowski, M. Aflatoxin B(1) Degradation by Ery4 Laccase: From In Vitro to Contaminated Corn. *Toxins* **2023**, *15* (5), 310.
(27) Sun, Z.; You, Y.; Xu, H.; You, Y.; He, W.; Wang, Z.; Li, A.; Xia, Y. Food-Grade Expression of Two Laccases in Pichia pastoris and Study on Their Enzymatic Degradation Characteristics for Mycotoxins. *J. Agric. Food Chem.* **2024**, *72* (16), 9365−9375.
(28) Lin, M.-I.; Nagata, T.; Katahira, M. High yield production of fungal manganese peroxidases by E. coli through soluble expression, and examination of the activities. *Protein Expression Purif.* **2018**, *145*, 45−52.
(29) Esakkimuthu, E. S.; Ponnuchamy, V.; Mikuljan, M.; Schwarzkopf, M.; Devallance, D. Fungal enzyme degradation of lignin-PLA composites: Insights from experiments and molecular docking simulations. *Heliyon* **2024**, *10* (1), No. e23838.
(30) Liu, Y.; Mao, H.; Hu, C.; Tron, T.; Lin, J.; Wang, J.; Sun, B. Molecular docking studies and in vitro degradation of four aflatoxins (AFB1, AFB2, AFG1, and AFG2) by a recombinant laccase from Saccharomyces cerevisiae. *J. Food Sci.* **2020**, *85* (4), 1353−1360.
(31) Yang, C.; Zhang, Z.; Peng, B. New insights into searching patulin degrading enzymes in Saccharomyces cerevisiae through proteomic and molecular docking analysis. *Journal of Hazardous Materials* **2024**, *463*, No. 132806.
(32) Qin, X.; Sun, X.; Huang, H.; Bai, Y.; Su, X. Oxidation of a non-phenolic lignin model compound by two Irpex lacteus manganese peroxidases: evidence for implication of carboxylate and radicals. *Biotechnol. Biofuels* **2017**, *10*, 103.
(33) Wang, X.; Qin, X.; Hao, Z.; Luo, H.; Su, X. Degradation of Four Major Mycotoxins by Eight Manganese Peroxidases in Presence of a Dicarboxylic Acid. *Toxins* **2019**, *11* (10), 566.
(34) Eberhardt, J.; Santos-Martins, D.; Tillack, A. F.; Forli, S. AutoDock Vina 1.2.0: New Docking Methods, Expanded Force Field, and Python Bindings. *J. Chem. Inf Model* **2021**, *61* (8), 3891−3898.
(35) Trott, O.; Olson, A. J. AutoDock Vina: improving the speed and accuracy of docking with a new scoring function, efficient optimization, and multithreading. *J. Comput. Chem.* **2010**, *31* (2), 455−461.
(36) Schein, C. H.; Noteborn, M. H. M. Formation of Soluble Recombinant Proteins in Escherichia Coli is Favored by Lower Growth Temperature. *Nat. Biotechnol.* **1988**, *6* (3), 291−294.
(37) Qing, G.; Ma, L. C.; Khorchid, A.; Swapna, G. V. T.; Inouye, M. Cold-shock induced high-yield protein production in *Escherichia coli*. *Nat. Biotechnol.* **2004**, *22* (7), 877−882.
(38) You, Y.; Qiu, Y.; Xu, H.; He, R.; Zhang, L.; Wang, Z.; Xia, Y. Effective and food-grade detoxification of multiple mycotoxins using yeast expressed manganese peroxidases. *Food Bioscience* **2024**, *59*, No. 103886.
(39) Gao, M. J.; Zhan, X. B.; Gao, P.; Zhang, X.; Dong, S. J.; Li, Z.; Shi, Z. P.; Lin, C. C. Improving Performance and Operational Stability of Porcine Interferon-α Production by Pichia pastoris with Combinational Induction Strategy of Low Temperature and Methanol/Sorbitol Co-feeding. *Appl. Biochem. Biotechnol.* **2015**, *176* (2), 493−504.
(40) Margawati, E. T.; Fuad, A. M.; Indriawati; Ridwan, M.; Volkandari, S. D. Optimization of expression JTAT protein with emphasis on transformation efficiency and IPTG concentration. *Journal of Genetic Engineering and Biotechnology* **2017**, *15* (2), 515−519.
(41) Studier, F. W. Use of T7 RNA polymerase to direct expression of cloned genes. *Methods Enzymol.* **1990**, *185*, 60−89.
(42) Chinnadurai, D.; Nallal, M.; Kim, H. J.; Li, O. L.; Park, K. H.; Prabakar, K. Mn3+ Active Surface Site Enriched Manganese Phosphate Nano-polyhedrons for Enhanced Bifunctional Oxygen Electrocatalyst. *ChemCatChem.* **2020**, *12* (8), 2348−2355.
(43) Whitwam, R.; Tien, M. Heterologous Expression and Reconstitution of Fungal Mn Peroxidase. *Archives of Biochemistry & Biophysics* **1996**, *333* (2), 439−446.
(44) Honda, H. C.; Kuwahara, W. Production of manganese peroxidase by pellet culture of the lignin-degrading basidiomycete Pleurotus ostreatus. *Appl. Microbiol. Biotechnol.* **2001**, *55*, 704−711.
(45) Shu, G.; Cheng, J.; Ting, Z.; Junxia, L.; Qiugang, M.; Tiangui, N. Aflatoxin B1 Degradation by Stenotrophomonas Maltophilia and Other Microbes Selected Using Coumarin Medium. *Int. J. Mol. Sci.* **2008**, *9* (8), 1489−1503.

https://doi.org/10.1021/acs.jafc.4c10047
J. Agric. Food Chem. 2025, 73, 1608−1618

(46) Xia, Y.; He, R.; Sun, Y.; Zhou, H.; Gao, M.; Hu, X.; Cui, X.; Cheng, Q.; Wang, Z. Food-Grade Expression of Manganese Peroxidases in Recombinant. *Frontiers in microbiology* **2022**, *12*, No. 821230.
(47) Chen, R. Bacterial expression systems for recombinant protein production: E. coli and beyond. *Biotechnology Advances* **2012**, *30* (5), 1102−1107.
(48) Sargsyan, K.; Grauffel, C.; Lim, C. How Molecular Size Impacts RMSD Applications in Molecular Dynamics Simulations. *J. Chem. Theory Comput.* **2017**, *13* (4), 1518−1524.
(49) Guterres, H.; Im, W. Improving Protein-Ligand Docking Results with High-Throughput Molecular Dynamics Simulations. *J. Chem. Inf. Model.* **2020**, *60*, 2189−2198.

https://doi.org/10.1021/acs.jafc.4c10047
J. Agric. Food Chem. 2025, 73, 1608−1618